Supporting Information

MOF-74 derived porous hybrid metal oxides hollow nanowires for high-performance electrochemical energy storage

Cuiping Yu[a,†], Yan Wang[a,b,†], Jiewu Cui[a,b,d*], Dongbo Yu[a,b], Xinyi Zhang[c], Xia Shu[a,b], Jianfang Zhang[a], Yong Zhang[a,b], Robert Vajtai[d], Pulickel M. Ajayan[d,*], Yucheng Wu[a,b,*]

[a] School of Materials Science and Engineering, Hefei University of Technology, Hefei, 230009, China

[b] Key Laboratory of Advanced Functional Materials and Devices of Anhui Province, Hefei, 230009, China

[c] School of Chemistry, Monash University, Clayton, VIC 3800, Australia

[d] Department of Materials Science and Nanoengineering, Rice University, Houston, TX 77005, USA

Corresponding authors: E-mails: jwcui@hfut.edu.cn, ajayan@rice.edu, ycwu@hfut.edu.cn

† These authors contributed equally to this work.

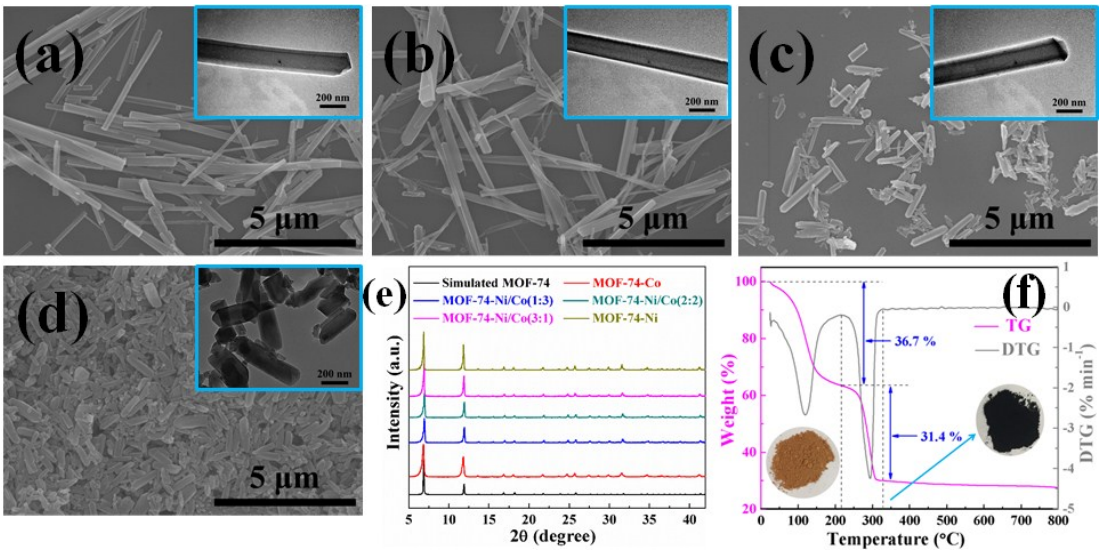

Fig. S1 FESEM images of MOF-74 with different Ni/Co concentration ratios (a) MOF-74-Co, (b) MOF-74-Ni/Co(1:3), (c) MOF-74-Ni/Co(3:1), (d) MOF-74-Ni (the insets refer to their corresponding TEM images), (e) XRD pattern and (f) TGA and DTG analysis of MOF-74 in air (the insets show the optical photographs of MOF-74 and metal oxides).

The phases of the as-prepared nanomaterials are confirmed by XRD pattern, all peaks are in line with those of the simulated MOF-74 XRD pattern, as shown in **Fig. S1e**, indicating the successful synthesis of MOF-74. And in order to obtain metal oxides from these five different kinds of MOF-74 materials, thermogravimetric analysis (TGA) and derivative thermogravimetric analysis (DTG) of MOF-74 in air are performed to research its decomposition process from room temperature to 800 ºC. In **Fig. S1f**, it is clear to see that there are two obvious stages of rapid weight loss, the first step of weight loss is about 36.7 %, which is attributed to the removal of water molecules in MOF-74 and the absorbed water, and the second one occurs at about 330 ºC with 31.4 % weight loss, which refers to the decomposition of the organic species, resulting in the formation of black metal oxides powders from the initial earth yellow

MOF-74 counterparts, it can be emphasized that its thermal stability is started from approximate 330 °C. Therefore, based on TGA result, 350 ºC is selected as the calcination temperature to accomplish the transformation of MOF-74 to metal oxide materials.

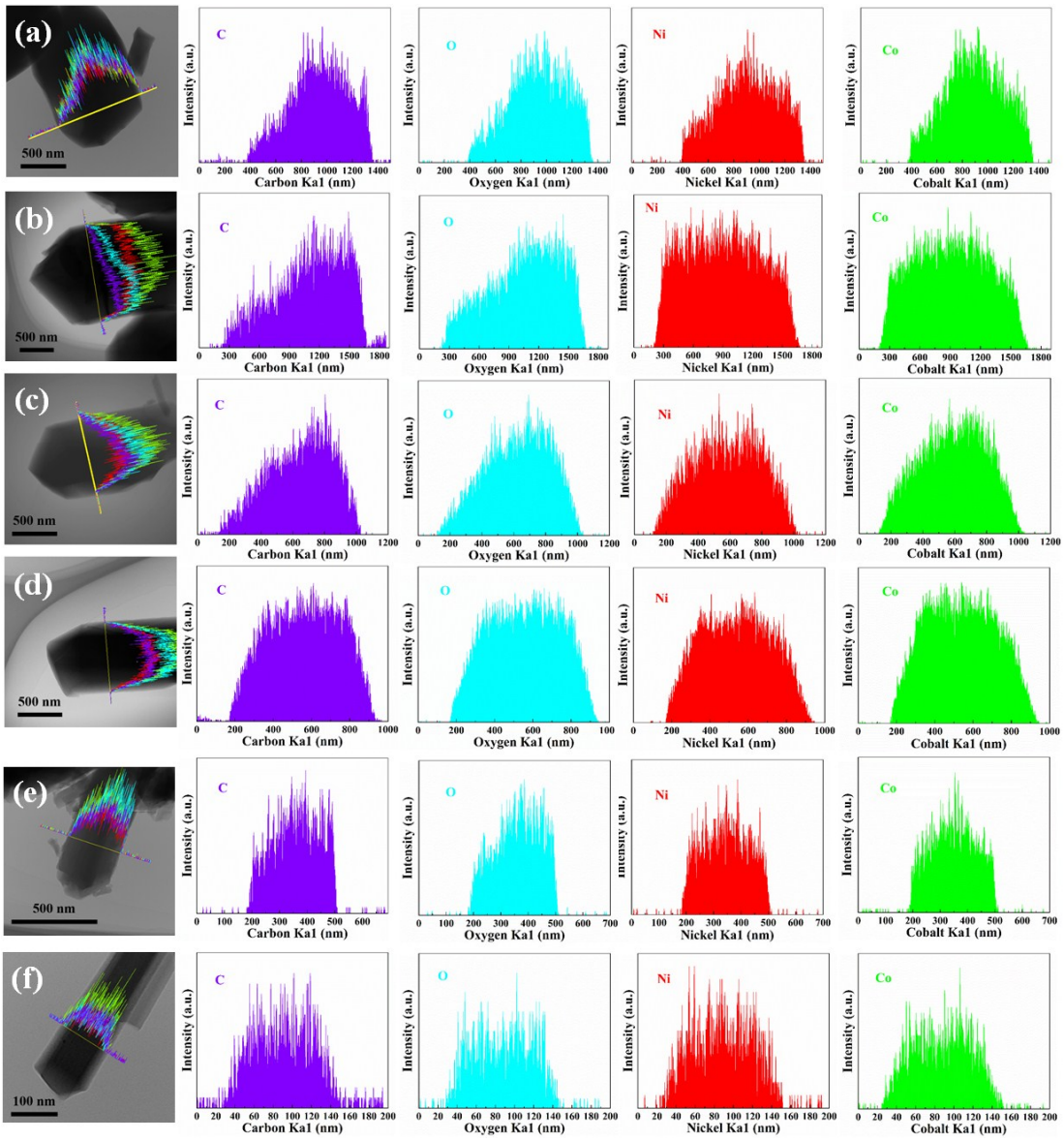

Fig. S2 EDX line scan analyses of MOF-74 with different ethanol/water volume ratios: (a) 1:1, (b) 1:2, (c) 1:3, (d) 1:4, (e) 1:5, (f) pure water without ethanol (MOF-74-Ni/Co(2:2)).

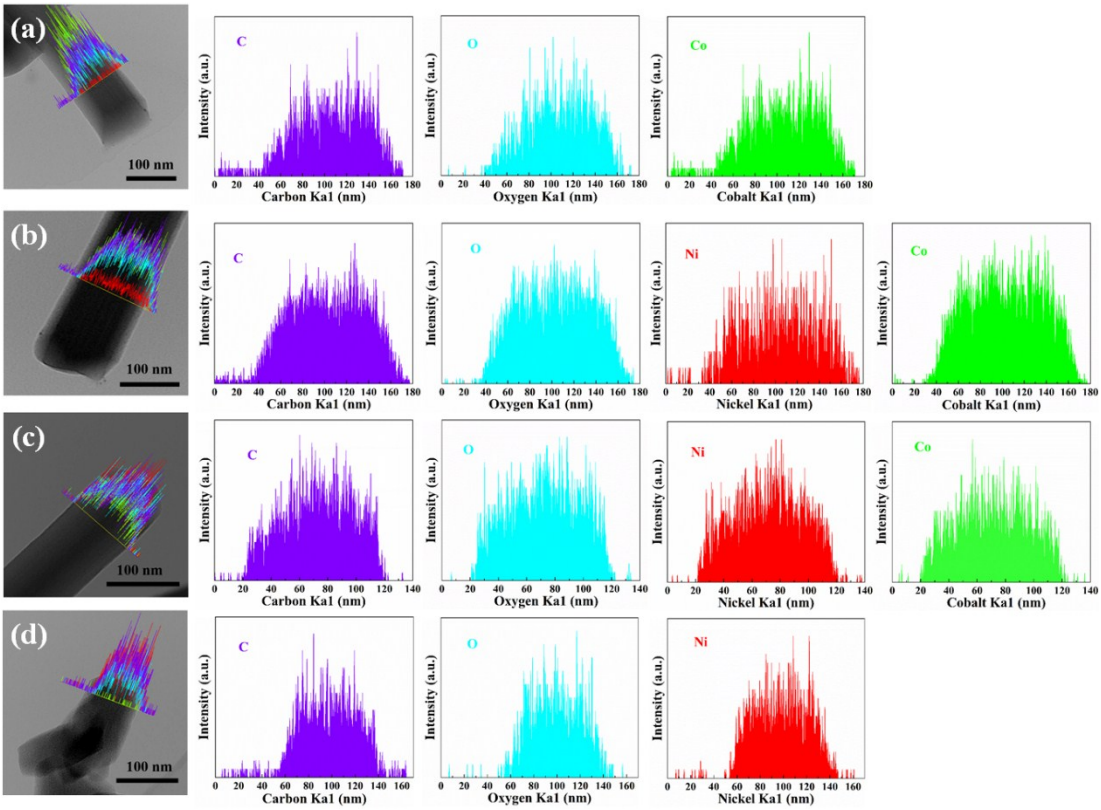

Fig. S3 EDX line scan analyses of MOF-74 nanowire with different Ni/Co concentration ratios: (a) MOF-74-Co, (b) MOF-74-Ni/Co(1:3), (c) MOF-74-Ni/Co(3:1), (d) MOF-74-Ni.

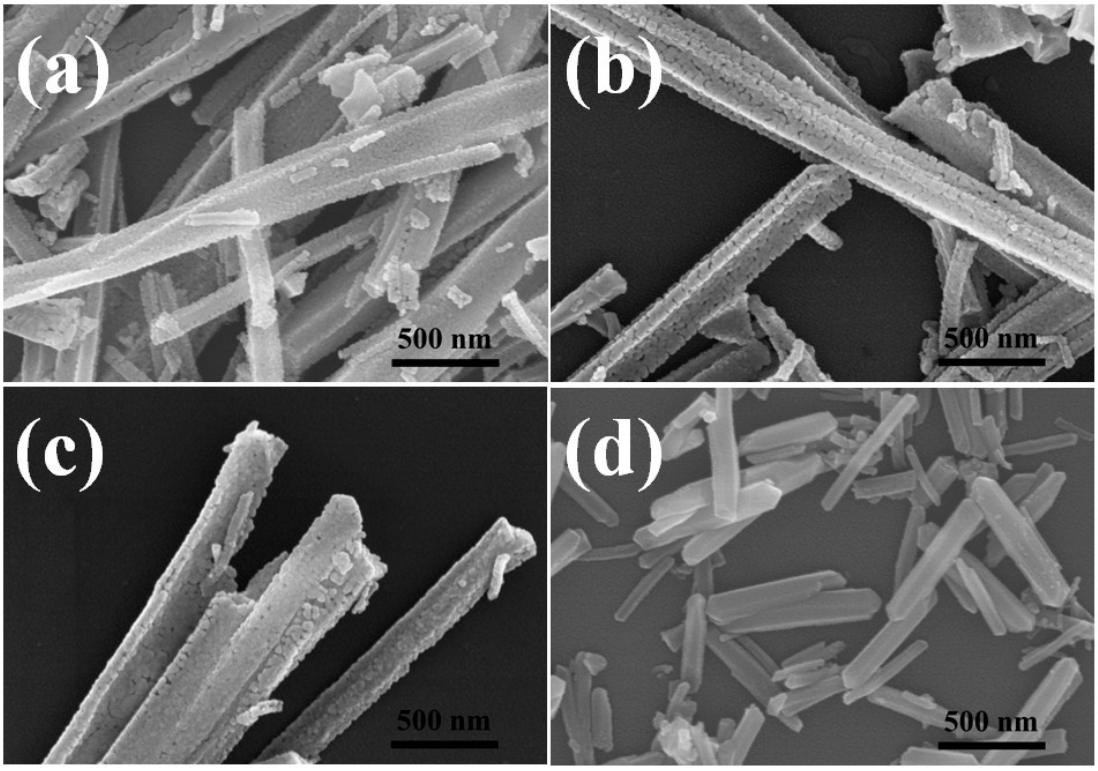

Fig. S4 FESEM images of the metal oxides (a) Co_3O_4, (b) $Co_3O_4/NiCo_2O_4$, (c)$NiO/NiCo_2O_4$(3.8:1) and (d) NiO.

Table S1. Atomic percentage of C, O, Ni and Co in metal oxides from XPS.

Precursor	C (at. %)	O (at. %)	Ni (at. %)	Co (at. %)	Ni/Co ratio	Final products
MOF-74-Ni/Co(1:3)	14.90	62.08	5.68	17.33	~1:3.0	$Co_3O_4/NiCo_2O_4$
MOF-74-Ni/Co(2:2)	15.52	60.48	12.29	11.70	~1:1.0	$NiO/NiCo_2O_4$(1:1)
MOF-74-Ni/Co(3:1)	13.50	59.41	19.17	7.91	~2.4:1	$NiO/NiCo_2O_4$(3.8:1)

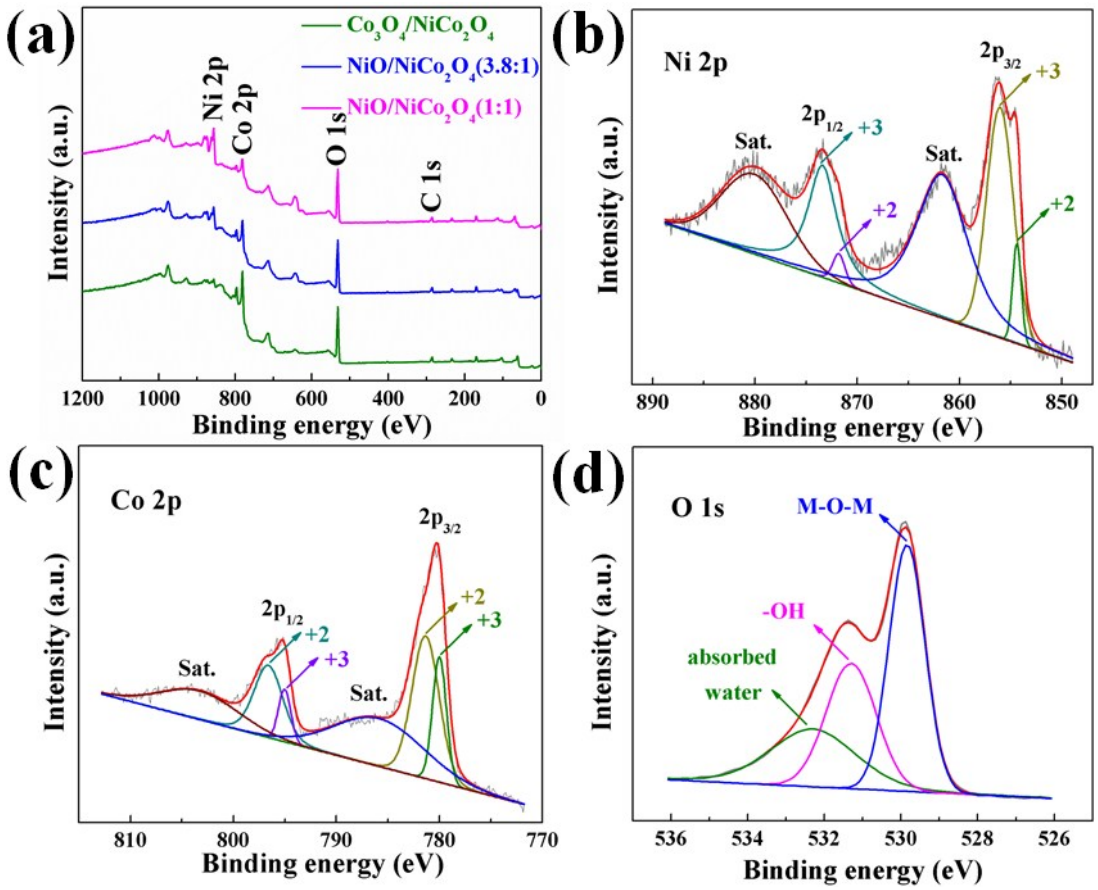

Fig. S5 (a) Full spectra of $Co_3O_4/NiCo_2O_4$, $NiO/NiCo_2O_4$(3.8:1) and $NiO/NiCo_2O_4$(1:1), (b) Ni 2p, (c) Co 2p and (d) O 1s of $NiO/NiCo_2O_4$(1:1).

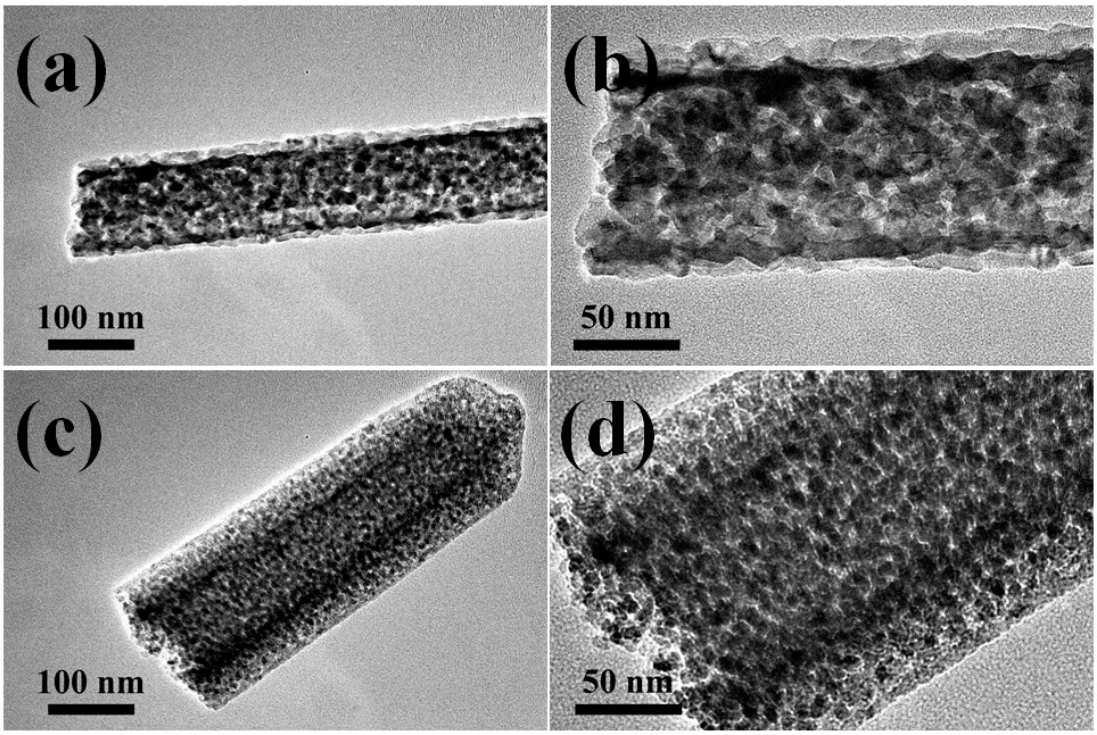

Fig. S6 TEM images of (a-b) $Co_3O_4/NiCo_2O_4$, (c-d) $NiO/NiCo_2O_4$(3.8:1).

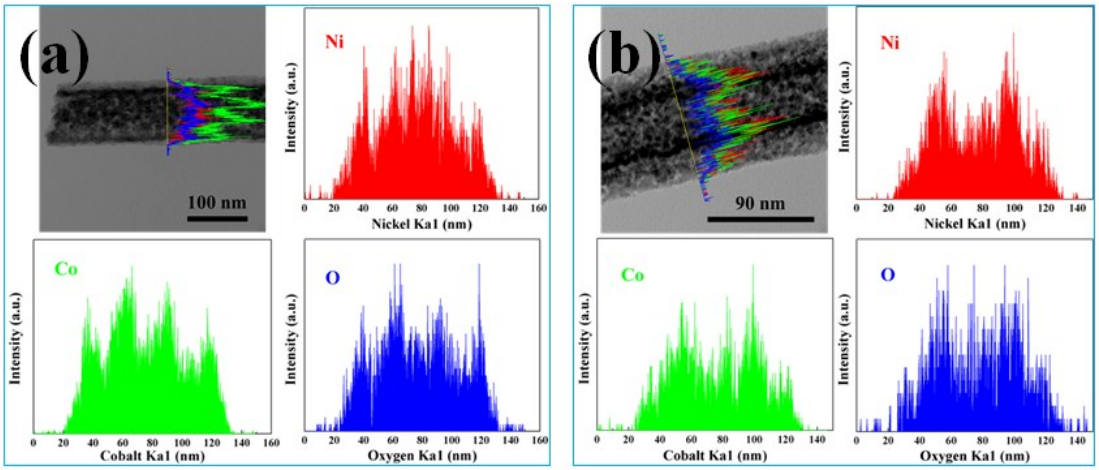

Fig. S7 EDX line scan analyses of (a) $Co_3O_4/NiCo_2O_4$ and (b) $NiO/NiCo_2O_4$(3.8:1).

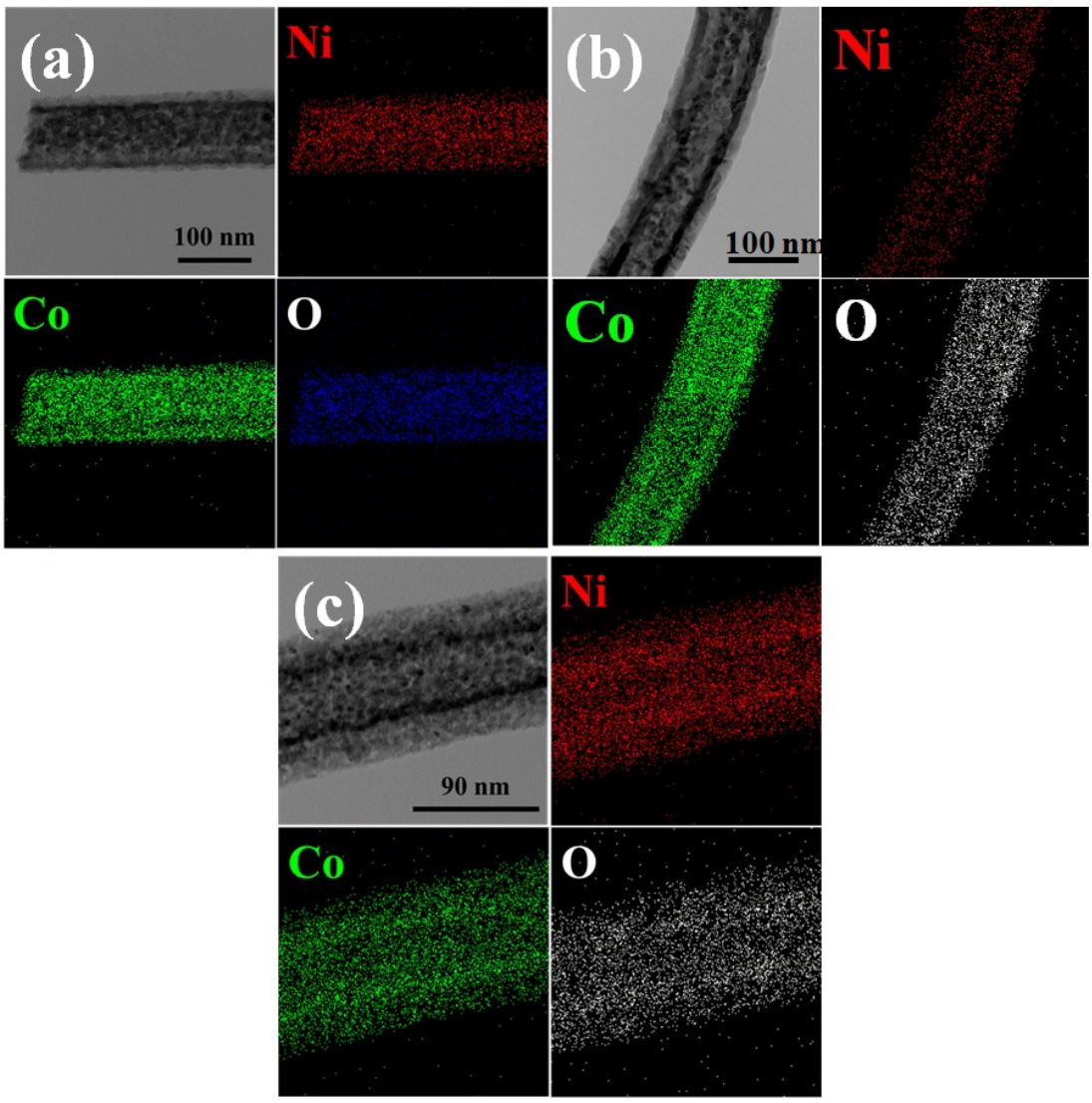

Fig. S8 EDX mapping analyses of (a) $Co_3O_4/NiCo_2O_4$, (b) $NiO/NiCo_2O_4$(1:1) and (c) $NiO/NiCo_2O_4$(3.8:1).

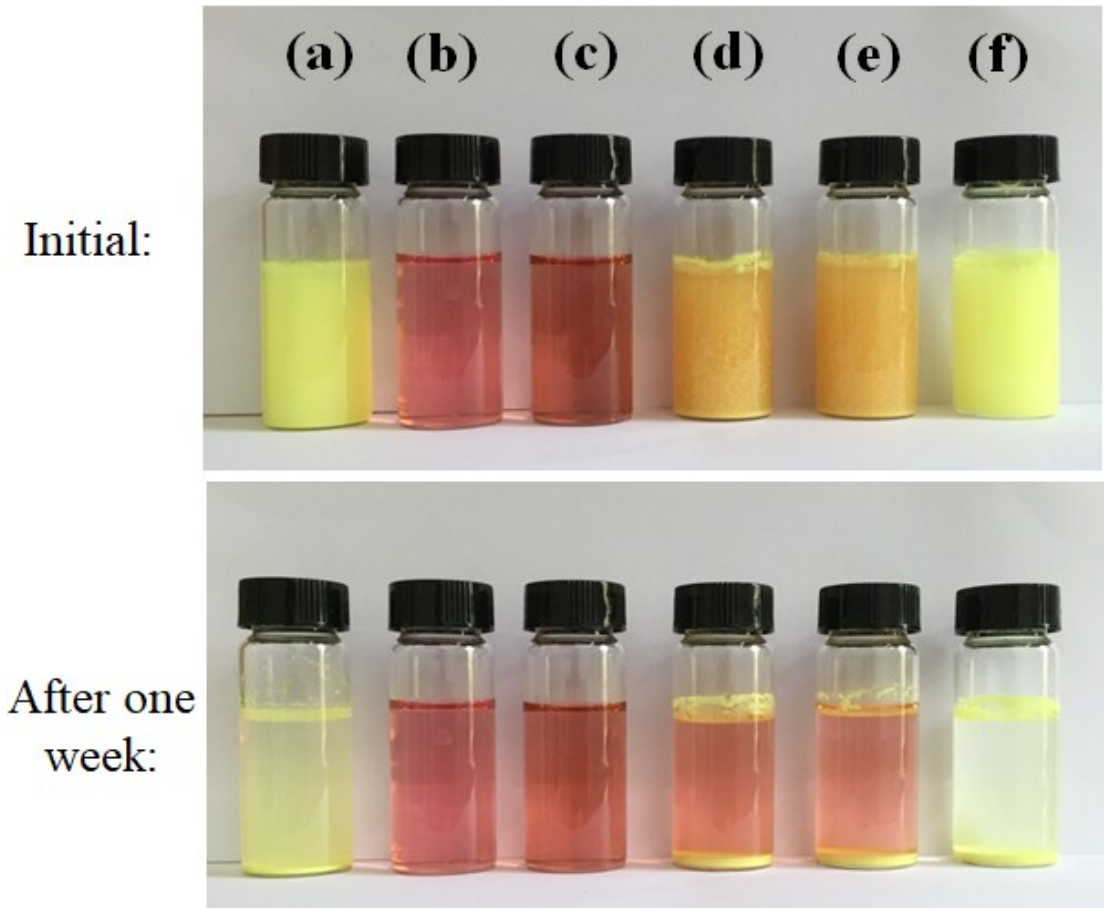

Fig. S9 (a) DHTA in water, (b) $Co(CH_3COO)_2$ aqueous solution, (c) DHTA in $Co(CH_3COO)_2$ aqueous solution, (d) DHTA in $Co(NO_3)_2$ aqueous solution, (e) DHTA in $CoCl_2$ aqueous solution, (f) DHTA in pure acetic acid aqueous solution.

As expected, DHTA could not dissolve in water, but it is interesting that when it mixes with acetate at room temperature, they could form the homogenous and transparent aqueous solution immediately, and the mechanism for this phenomenon is further investigated. Firstly, the same amount of DHTA is added into different kinds of aqueous solutions, as shown in **Fig. S9**. Obviously, DHTA is insoluble in $Co(NO_3)_2$ or $CoCl_2$ aqueous solutions compared with $Co(CH_3COO)_2$ aqueous solution, in addition, DHTA could not dissolve in pure acetic acid aqueous solution. The reason for this phenomenon is ascribed to acidity of DHTA [pKa<2.97] is stronger than that of acetic acid [pKa=4.74] but weaker than that of nitric acid [pKa=-1.3] and hydrochloric acid [pKa=-8]. When salt acetate solution was added in DHTA suspension, acetate captured the protons from DHTA. During this process, DHTA lost protons and became water soluble ionic compound. What's more, there is no precipitate obtained even after one week as shown in **Fig. S9**, suggesting that the synthesis process of MOF-74 needs high temperature rather than room temperature. And secondly, NaOH aqueous solutions with

different concentrations are prepared to research the solubility of DHTA in alkaline aqueous solution. As shown in **Fig. S10**, the solubility of DHTA increases with the increasing of NaOH concentration, and it could dissolve completely with NaOH concentration larger than 40 mM. And the reason is that protons in DHTA are captured by strong OH^- in alkaline solution and DHTA formed water soluble ionic compound, which is similar to the function of salt acetate. And based on the transparent aqueous solution of DHTA in NaOH, 40 mM $CoCl_2$ is added, after reaction at 90 °C for 1 h, MOF-74 could be formed, and the corresponding morphology and XRD pattern are presented in **Fig. S11**, which is in great agreement with the aforementioned analysis in this paper.

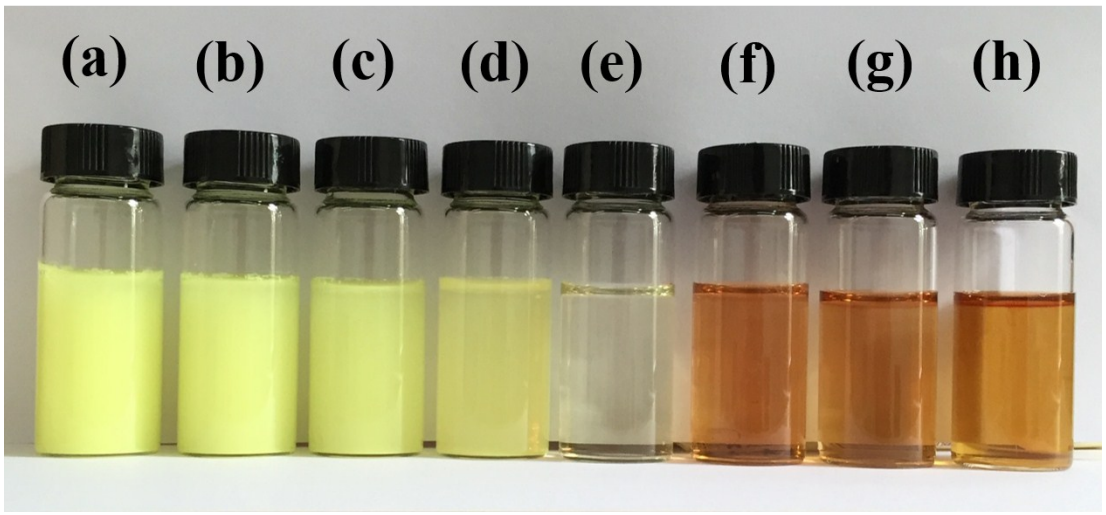

Fig. S10 DHTA in NaOH aqueous solution with different concentration: (a) 1 mM, (b) 10 mM, (c) 20 mM, (d) 30 mM, (e) 40 mM, (f) 50 mM, (g) 60 mM, (h) 80 mM.

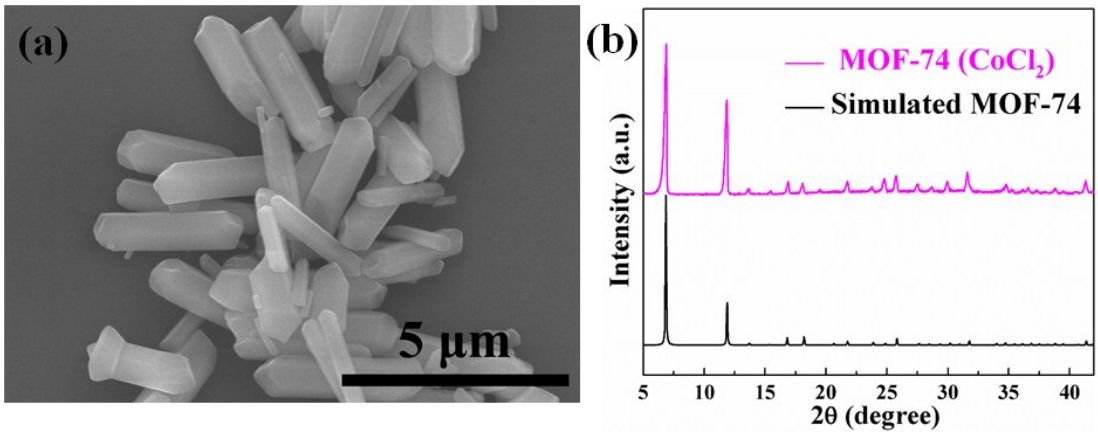

Fig. S11 (a) FESEM image and (b) XRD pattern of MOF-74 prepared by $CoCl_2$.

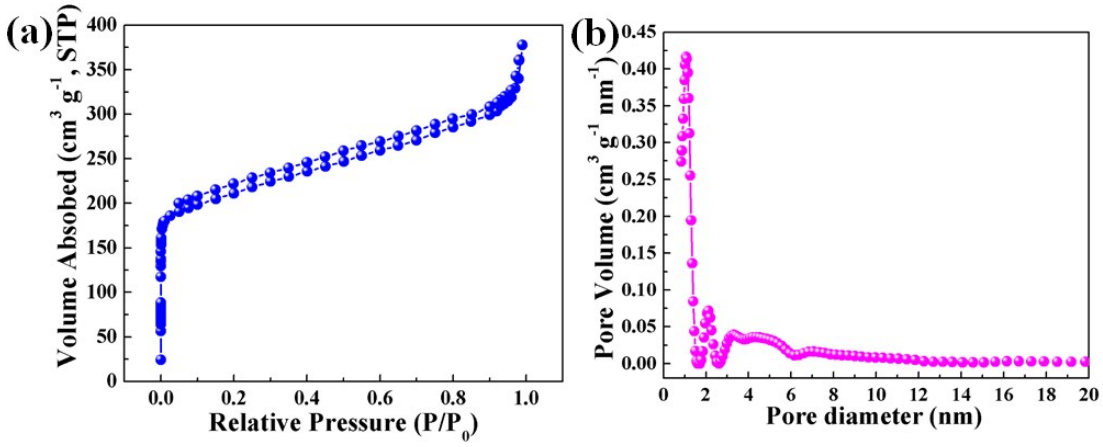

Fig. S12 (a) Nitrogen adsorption-desorption isotherm and (b) pore-size distribution of MOF-74-Ni/Co(2:2).

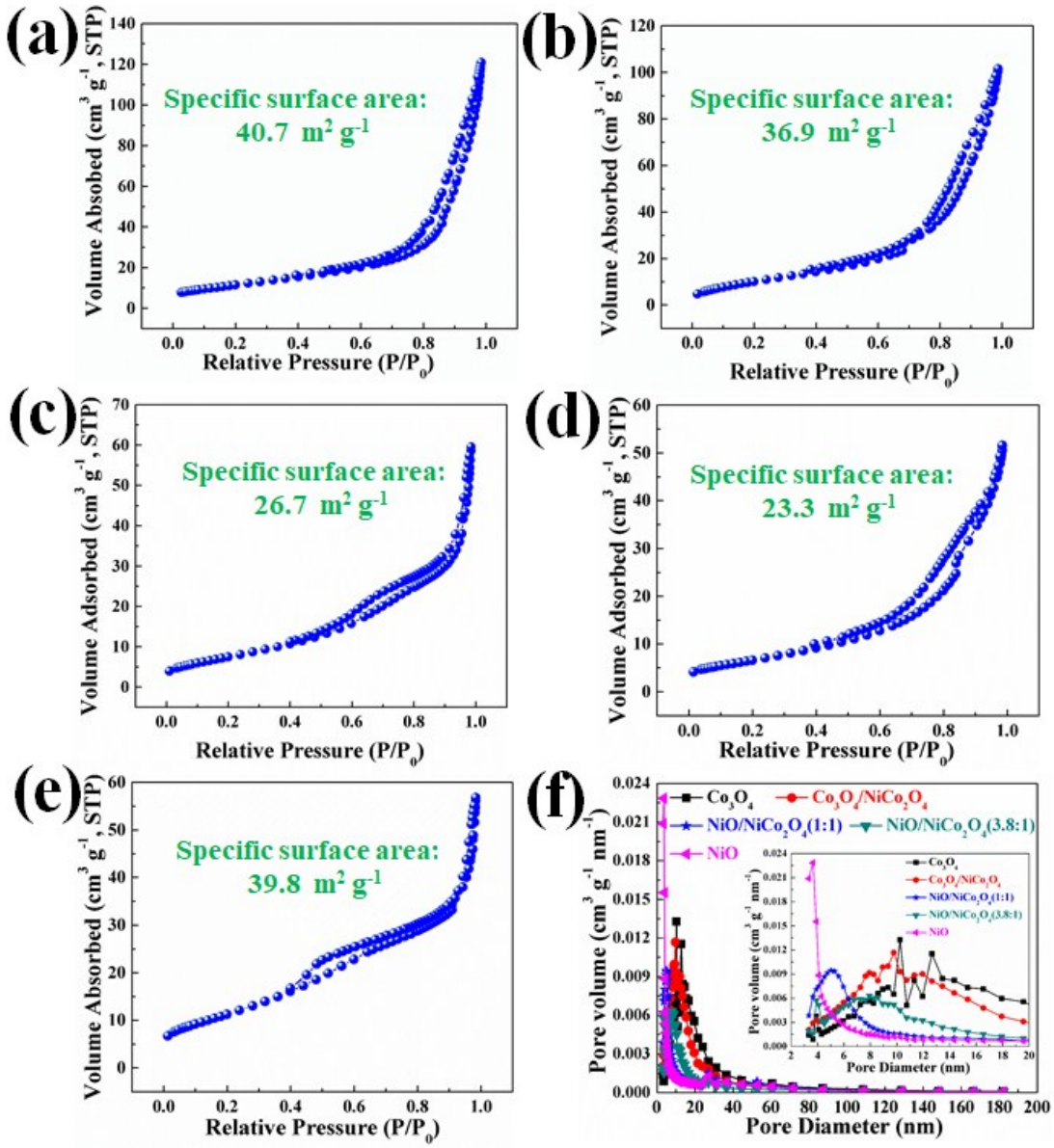

Fig. S13 Nitrogen adsorption-desorption isotherms of (a) Co_3O_4, (b) $Co_3O_4/NiCo_2O_4$, (c) $NiO/NiCo_2O_4$(1:1), (d) $NiO/NiCo_2O_4$(3.8:1) and (e) NiO, (f) pore size distributions of the as-prepared five different kinds of metal oxides.

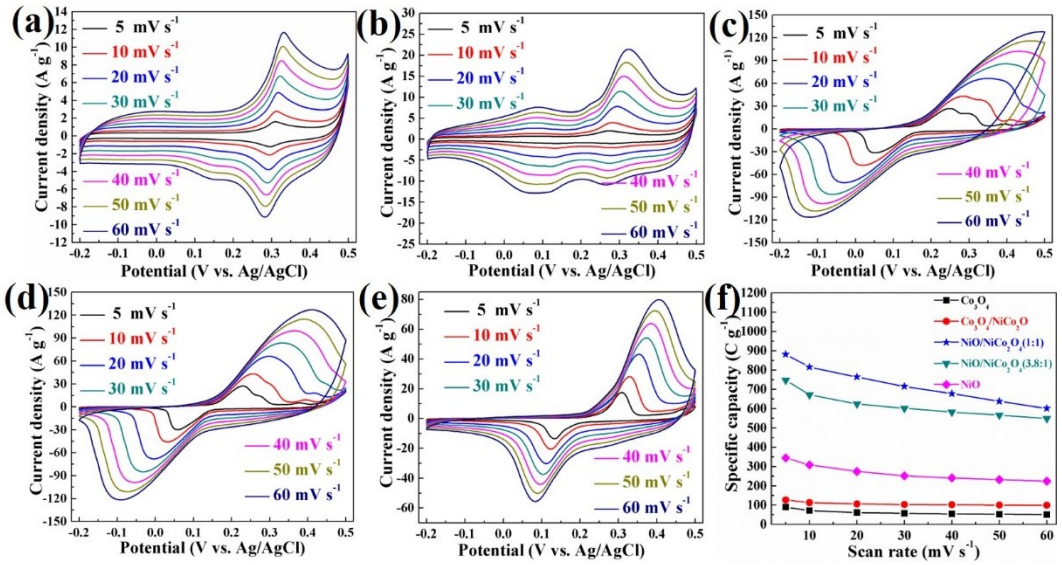

Fig. S14 CV curves of (a) Co_3O_4, (b) $Co_3O_4/NiCo_2O_4$, (c) $NiO/NiCo_2O_4$(1:1), (d) $NiO/NiCo_2O_4$(3.8:1) and (e) NiO at different scan rates ranging from 5 to 60 mV s^{-1}, (f) specific capacity calculated from CV curves.

Table S2 Charge storage mechanisms of Co_3O_4, $Co_3O_4/NiCo_2O_4$, $NiO/NiCo_2O_4$(3.8:1) and NiO.

Sample	Charge storage mechanism
Co_3O_4	$Co_3O_4 + H_2O + OH^- \leftrightarrow 3CoOOH + e^-$ $CoOOH + OH^- \leftrightarrow CoO_2 + H_2O + e^-$
$Co_3O_4/NiCo_2O_4$	$Co_3O_4 + H_2O + OH^- \leftrightarrow 3CoOOH + e^-$ $NiCo_2O_4 + OH^- + H_2O \leftrightarrow NiOOH + 2CoOOH + e^-$ $CoOOH + OH^- \leftrightarrow CoO_2 + H_2O + e^-$
$NiO/NiCo_2O_4$(3.8:1)	$NiO + OH^- \leftrightarrow NiOOH + e^-$ $NiCo_2O_4 + OH^- + H_2O \leftrightarrow NiOOH + 2CoOOH + e^-$ $CoOOH + OH^- \leftrightarrow CoO_2 + H_2O + e^-$
NiO	$NiO + OH^- \leftrightarrow NiOOH + e^-$

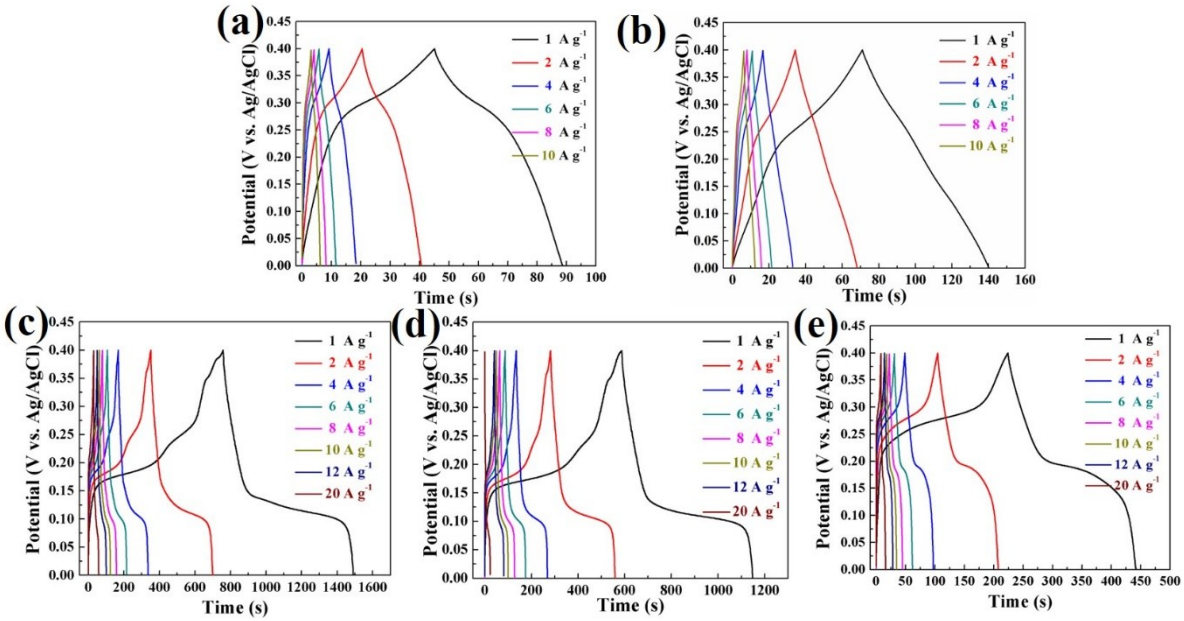

Fig. S15 GCD curves of (a) Co_3O_4, (b) $Co_3O_4/NiCo_2O_4$, (c) $NiO/NiCo_2O_4$(1:1), (d) $NiO/NiCo_2O_4$(3.8:1) and (e) NiO at different current densities.

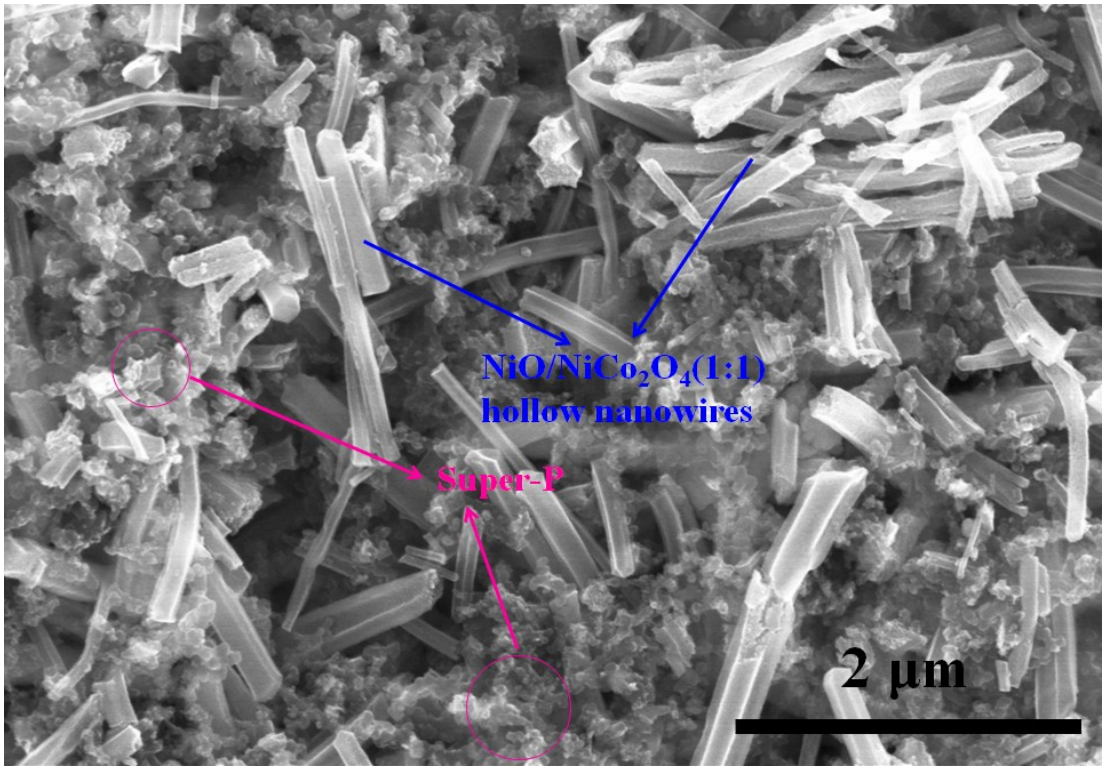

Fig. S16 FESEM image of positive electrode after cycling for 3000 cycles.

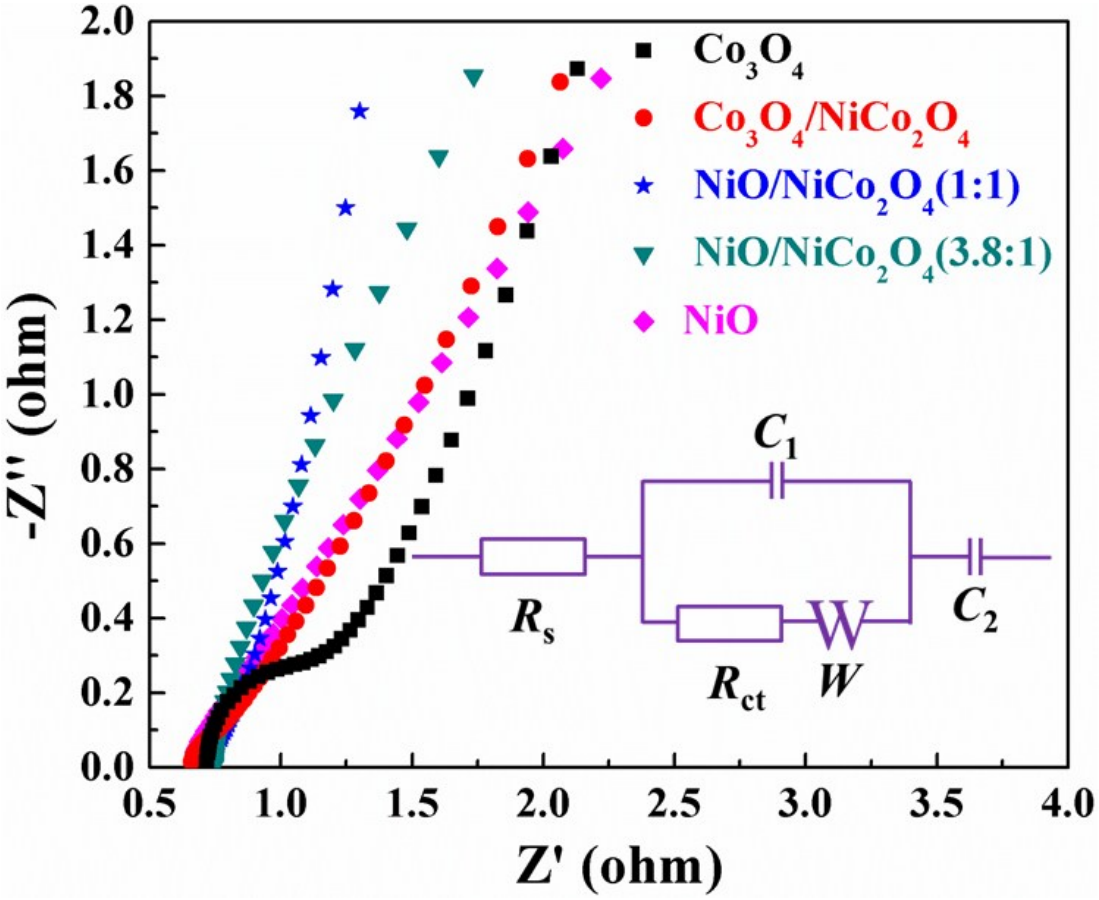

Fig. S17 Nyquist plots of the as-prepared five electrodes after fitting (the inset shows the fitting equivalent electrical circuit).

Table S3 Comparison of electrochemical properties based on nickel cobalt oxides-based and MOFs-derived materials.

Electrode materials	Precursor	Synthesis solvent	Synthesis Approach	Specific capacity (C g^{-1})	Specific capacitance (F g^{-1})	Ref.
$NiO/NiCo_2O_4$ (1:1) hollow nanowires	MOF-74	Water	90 ºC oil bath reaction for 1 h	732.0 (1.0 A g^{-1})	1830.0	This work
$Ni_xCo_{3-x}O_4$-1 nanoparticles	MOF-74	DMF-ethanol-water with volume ratio of 1:1:1	100 ºC hydrothermal for 24 h	398.5 (1.0 A g^{-1})	797.0	1
$NiCo_2O_4$@CNTs	CoO+$Ni(OH)_2$NiOOH	water	Precipitation	636.0 (0.5 A g^{-1})	1590.0	2
Co_3O_4 Nanosheets	Co-based MOF (UPC-9)	DMA-H_2O with volume ratio of 1:1	120 °C hydrothermal for 3 days	616.6 (1.0 A g^{-1})	1121.0	3
Co_3O_4 nanoparticles	Co-MOF	H_2O-CH_3CN with volume ration of 3:1	140 ºC hydrothermal for 72 h	68.6 (0.5 A g^{-1})	137.2	4
NiO nanospheres	Ni-MOF	DMF-EG with volume ration of 20:6	120 ºC hydrothermal for 6 h	212.9 (0.5 A g^{-1})	473.0	5
NiO nanosheets	α-$Ni(OH)_2$	Methanol-water-EG with volume ratio of 32.9:2:26	Aging for 2 days and 170 ºC hydrothermal for 5 h	183.2 (1 A g^{-1})	407.0	6
$NiCo_2O_4$nanosheets	(Co, Ni)O(OH)	Methanol-water-EG with volume ratio of 32.9:2:26	Aging for 2 days and 170 ºC hydrothermal for 24 h	394.2 (1 A g^{-1})	876.0	6
Ni_2CoS_4@$NiCo_2O_4$/CFP	$NiCo_2O_4$ CFP	water	120 ºC hydrothermal for 16 h and electrodeposition	750.5 (1.0 mA cm^{-2})	1501.0	7
FCP-$NiCo_2O_4$/rGO/CNTs	-	water	Refluxing growth	809.0 (1 A g^{-1})	1618.0	8
$NiCo_2O_4$NWAs/Carbon Textiles	$NiCo_2(OH)_6$	water	100 ºC hydrothermal	512.0 (1 A g^{-1})	1283.0	9
$NiCo_2O_4$ nanowires	Nickel cobalt oxalate	Cyclohexane-n-pentanol-water	Microemulsion	- (1 A g^{-1})	1197.0	10

Note:
DMF: N,N-dimethylformamide, CNTs: carbon nanotubes, NS-C: carbon co-doped with N and S rGO: reduced Graphene Oxide, GO: Graphene Oxide, EG: ethylene glycol, CFP: carbon fiber paper, FCP: few-crystalline and porous, NWAs: Nanowire arrays

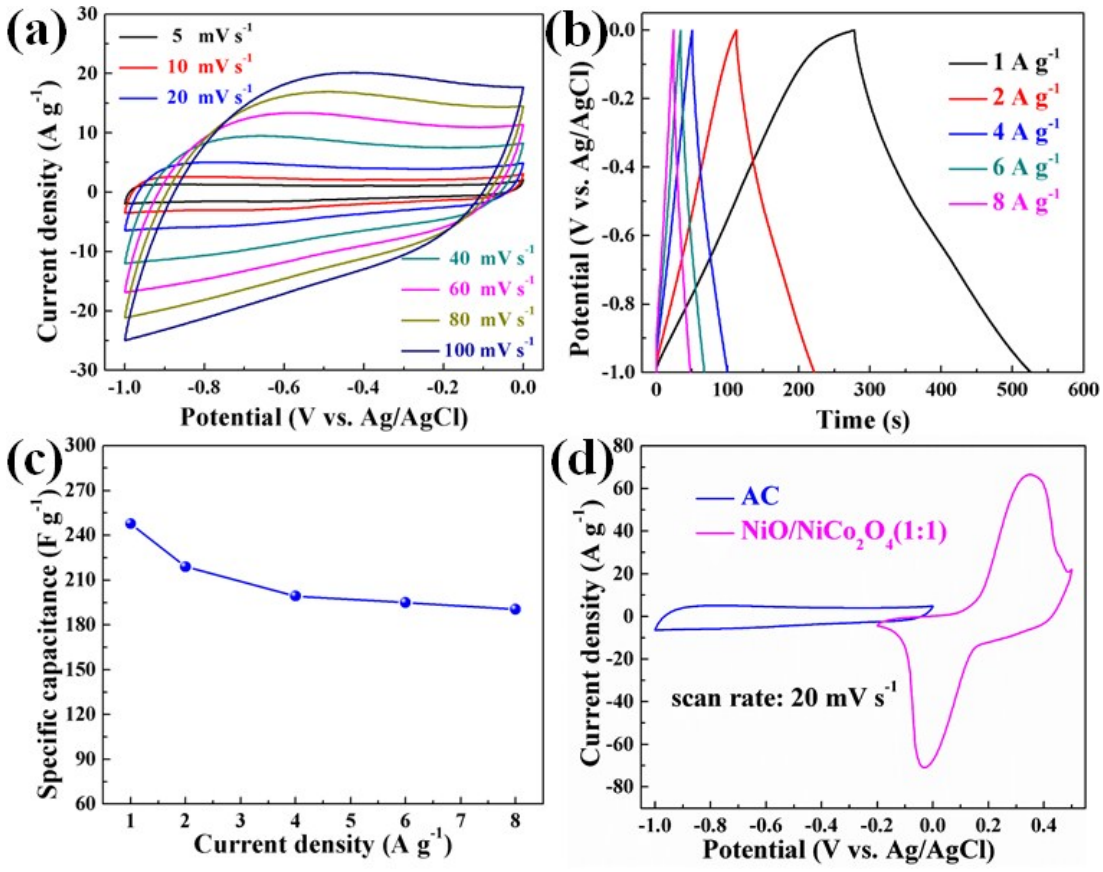

Fig. S18 (a) CV and (b) GCD curves of negative electrode, (c) specific capacitance at different current densities of the negative electrode, (d) CV curves of positive electrode and negative electrode at a scan rate of 20 mV s^{-1}.

The charge balance of the assembled supercapacitor devices is followed the relationship of $Q_+ = Q_-$, and $Q = C*m*\Delta E$, where C, m and ΔE refer to the specific capacitance (F g^{-1}), mass of the electrode (g), potential window of the charging/discharging process (V), respectively. Therefore, from the CV curves of positive and negative electrodes at the scan rate of 20 mV s^{-1} in Fig. S15d, the mass balancing m_+/m_- of $NiO/NiCo_2O_4$(1:1)//AC is calculated to be:

$$\frac{m_+}{m_-} = \frac{C_- * \Delta E_-}{C_+ * \Delta E_+} = \frac{208.8 * 1.0}{1091.2 * 0.7} = 0.273$$

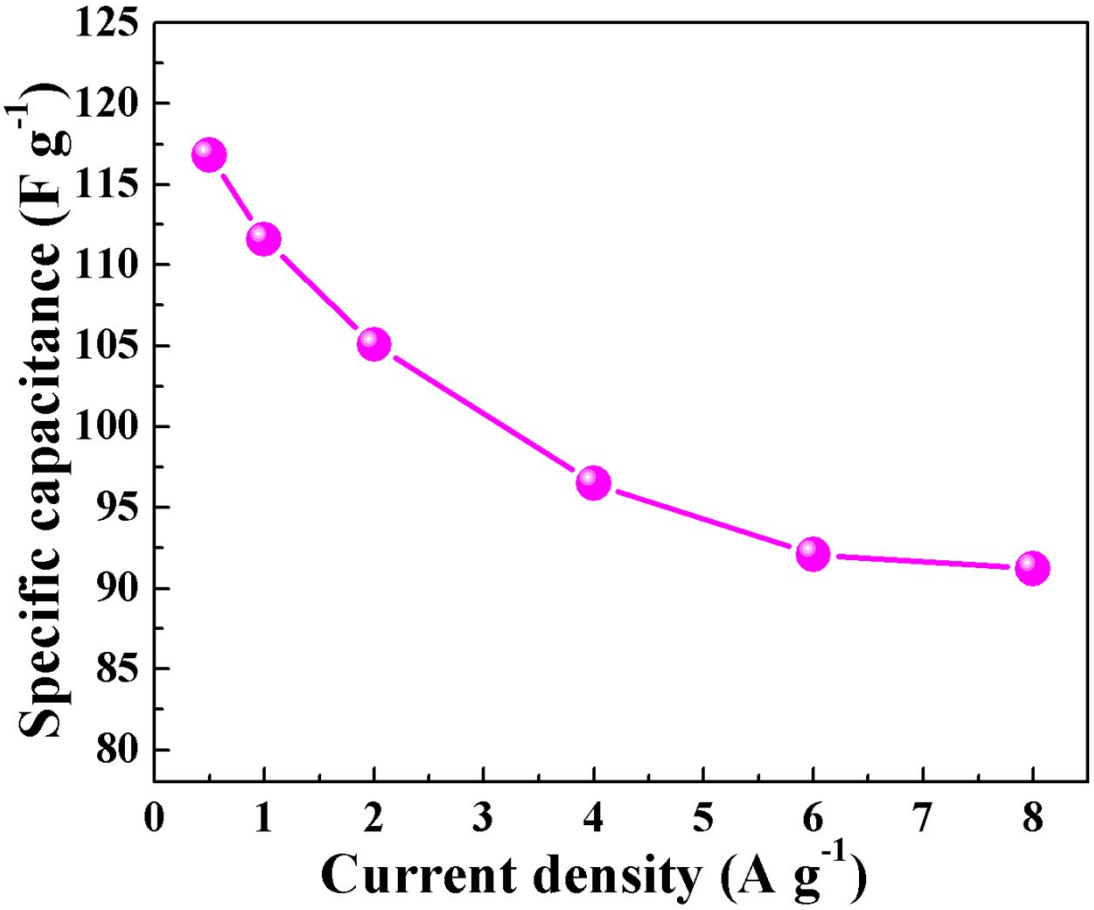

Fig. S19 Specific capacitance of $NiO/NiCo_2O_4$(1:1)//AC asymmetric supercapacitor device at different current densities.

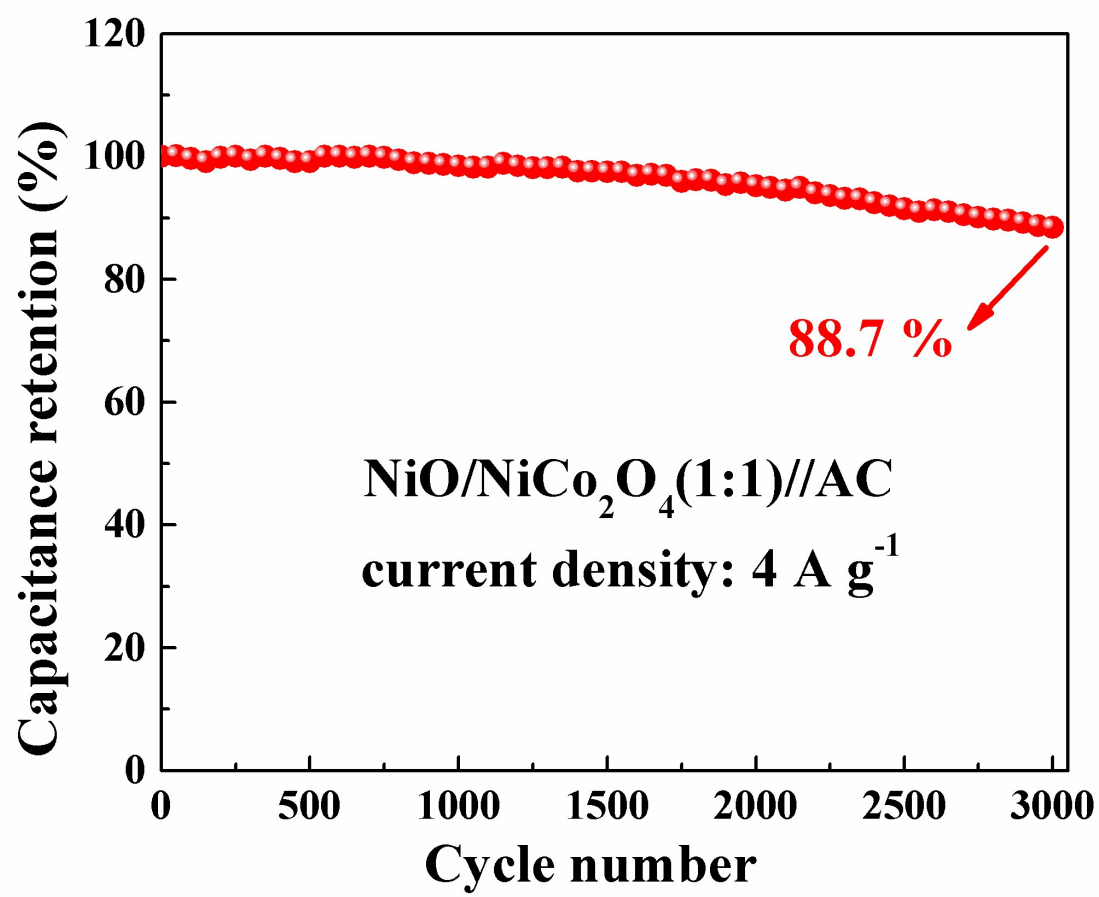

Fig. S20 Cycling performance of this asymmetric supercapacitor device at a current density of 4 A g^{-1} for 3000 cycles.

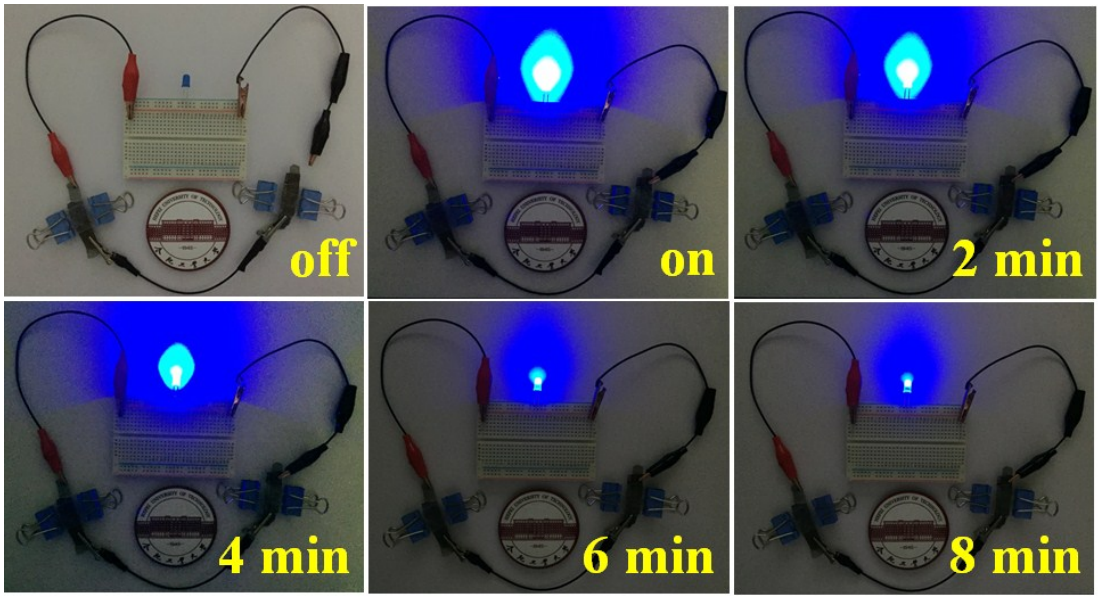

Fig. S21 Optical photographs of this kind of LED working at different time.

References

1 S. Chen, M. Xue, Y. Li, Y. Pan, L. Zhu, S. Qiu, *J. Mater. Chem. A*, 2015, **3**, 20145-20152.

2 P. Wu, S. Cheng, M. Yao, L. Yang, Y. Zhu, P. Liu, O. Xing, J. Zhou, M. Wang, H. Luo, M Liu, *Adv. Funct. Mater.*, 2017, **27**, 1702160.

3 Z. Xiao, L. Fan, B. Xu, S. Zhang, W. Kang, Z. Kang, H. Lin, X. Liu, S. Zhang, D. Sun, *ACS Appl. Mater. Interfaces*, 2017, **9**, 41827-41836.

4 F. Meng, Z. Fang, Z. Li, W. Xu, M. Wang, Y. Liu, J. Zhang, W. Wang, D. Zhao, X. Guo, *J. Mater.Chem. A*, 2013, **1**, 7235-7241.

5 M.-K. Wu, C. Chen, J.-J. Zhou, F.-Y. Yi, K. Tao, L. Han, *J. Alloy. Compd.*, 2018, **734**, 1-8.

6 L. Zhang, W. Zheng, H. Jiu, C. Ni, J. Chang, G. Qi, *Electrochim. Acta*, 2016, **215**, 212-222.

7 L. Cao, G. Tang, J. Mei, H. Liu, *J. Power Sources*, 2017, **359**, 262-269.

8 L. Zhang, L. Dong, M. Li, P. Wang, J. Zhang, H. Lu, *J. Mater. Chem. A*, 2018, **6**, 1412-1422.

9 L. Shen, Q. Che, H. Li, X. Zhang, *Adv. Funct. Mater.*, 2014, **24**, 2630-2637.

10 C. An, Y. Wang, Y. Huang, Y. Xu, L. Jiao, H. Yuan, *Nano Energy*, 2014, **10**, 125-134.